SIMULATION OF PUNCHING FAILURE: FAILURE MECHANISM AND SIZE-EFFECT

Ph. Menétrey,
Institut de Béton Armé et Précontraint (IBAP),
Ecole Polytechnique Fédérale de Lausanne (EPFL), Switzerland.

Abstract

Finite element simulation of punching failure in reinforced concrete structures is investigated. The non-linear material behavior is considered by superimposing the elastoplastic behavior of steel reinforcement and the tensile cracking behavior of concrete.

The simulation of punching failure is performed for a circular slab. It is shown that the punching mode of failure—characterized by a localized inclined crack—is reproduced. This simulation indicates that the failure mechanism results from micro-crack coalescence phenomenon at the top of the slab followed by a crack propagation towards the corner of the slab-column.

The size-effect is reproduced numerically. It is shown that a modification of the tensile stress distribution along the punching crack reflects the influence of the size. A size-effect law is proposed based on the adjustment of the numerical results.

1   Introductory remarks

Reinforced concrete slabs supported on columns fail by punching when a column suddenly perforates the slab by extrusion of a conical plug of concrete. A review of this failure phenomenon has been presented by Regan and Braestrup (1985). The approach adopted here is concerned with the numerical simulation of this failure mechanism. Further details are given by Menétrey et al. (1994), (1995a), and (1995b).

2   Numerical model

2.1   Preliminaries

The reinforced concrete model uncouples the actions of steel reinforcement and concrete. The incremental flow theory of plasticity is considered as the framework of the constitutive model description.

The steel model is characterized by a bi-linear stress-strain behavior and an identical response under traction and compression.

The concrete model is characterized by a triaxial strength which is delimited by a new 3-parameter failure criterion described by Menétrey and Willam (1995). A non-associated flow rule is derived so as to reproduce the dilatancy of the plastic strains observed in concrete triaxial experiments as reported by Menétrey et al. (1995a).

2.2   Concrete cracking simulation

The crack formation is described in a general manner with strain-softening which refers to a gradual decrease in tensile strength with additional deformation. The fictitious crack model developed by Hillerborg et al. (1976) is considered for which the tensile stress σ_t is controlled by the crack opening w. This mechanism is controlled by the degradation of the cohesive parameter c. The decohesion function is expressed with an exponential in order to fit the tensile experimental data which dominates the post-peak response of concrete

$$c = \frac{\sigma_t}{f_t} = \exp\left\{-a\frac{w}{w_r}\right\},\tag{1}$$

where a is the slope of the softening branch, f_t the tensile strength of concrete, and w_r the crack rupture opening. The concrete failure criterion is written so that the cohesive parameter is decoupled,

resulting in an isotropic loss of strength due to reduction of the cohesion.

The energy absorbed in the fracture zone to complete separation of the specimen in tension is expressed as

$$G_f = \int_0^{w_r} \sigma_t dw = \int_0^{w_r} f_t \exp\left\{-a\frac{w}{w_r}\right\} dw \approx \frac{f_t w_r}{a}, \qquad (2)$$

defining the fracture energy. The fracture energy must be invariant with the finite element size. Therefore, the mapping between the crack opening w used for the definition of the constant fracture energy, and the strain ϵ used at the constitutive level leads to the definition of the height of the element h^e normal to the crack band so that $w = h^e \epsilon$.

From experiments, it is known that tensile splitting in compression as well as shear is due to distributed micro-cracking. Hence, a general crack model can be interpreted as a multiple tensile crack model. Consequently, the fracture model for tension is extended to capture general fracture based on the definition of the fictitious number of cracks N which is formed in a specimen under a given state of stress.

The cracking phenomenon is also responsible for stiffness degradation and the model described by Lubliner et al. (1989) is considered. It is based on the assumption that elastic degradation occurs only in the softening range.

In order to evaluate the plastic corrector step, the cutting plane algorithm developed by Ortiz and Simo (1986) is used which is coupled to a relaxation method.

2.3   Finite element model

The analysis of circular concrete slabs is considered. The concrete is modelled with four node quadrilateral axisymmetric continuum elements. The size of the element (h^e) which appears in the softening formulation is the square root of the cross section area so that the radial direction is not taken into account. This implies that a constant crack spacing along the perimeter is simulated (observed experimentally during punching failure).

The developed concrete constitutive model often allows for little volume change, so if plastic strains become large, the response becomes nearly incompressible. This difficulty is overcome by the treatment of incompressibility as developed by Hughes (1980) using the mean-dilatation formulation.

The non-linear solution is advanced with incremental and iterative steps using the modified Newton-Raphson algorithm.

3 Failure mechanism

The circular slab tested by Kinnunen and Nylander (1960) and denoted by IB15a is simulated. This slab is considered because of its perfect axially symmetric geometry (circular reinforcement). It has a total diameter of 1840 mm and a thickness of 150 mm. Experimentally, the load is applied to the column (150 mm in diameter) by mean of a hydraulic jack and transferred to the floor by mean of 12 tie rods along a radius of 855 mm.

The cracking phenomenon in the vicinity of the column as shown in figure 1 for three load steps (the tangential cracks are symbolized with a straight line for which the length is proportional to (1-c) and the orientation equals the principal strains orientation). The first inclined stress-free crack ($c < 0.01$) appears inside the slab thickness, just below the reinforcement. Under increasing displacement, this inclined crack expands toward the corner of the slab-column and the micro-cracks around are closing. At failure, the punching crack has reached the corner of the slab-column and the slab is separated into two parts.

These plots illustrate that the punching failure results from micro-cracks coalescence at the top of the slab. This micro-cracks coalescence are further justified experimentally by the tests of Regan (1983) (micro-cracks are formed across the slab thickness before failure occurs) and Moe (1961) (formation of inclined cracks across the slab thickness before failure occurs). Micro-cracks coalescence is followed by a crack propagation at the bottom of the slab already suggested by the ACI committee 446 (1992). However, the proposed direction of propagation is the contrary to the one observed here as the punching crack is propagating from the upper part of the slab to the bottom.

4 Size-effect

The size-effect is studied for the same circular slab but made with orthogonal reinforcement (modelled with ring and axisymmetric bar elements). The partial bond between concrete and steel is simulated by fasten rigidly the steel to the concrete only at the extremity of a fictitious fastening length. The purpose of this fictitious fastening
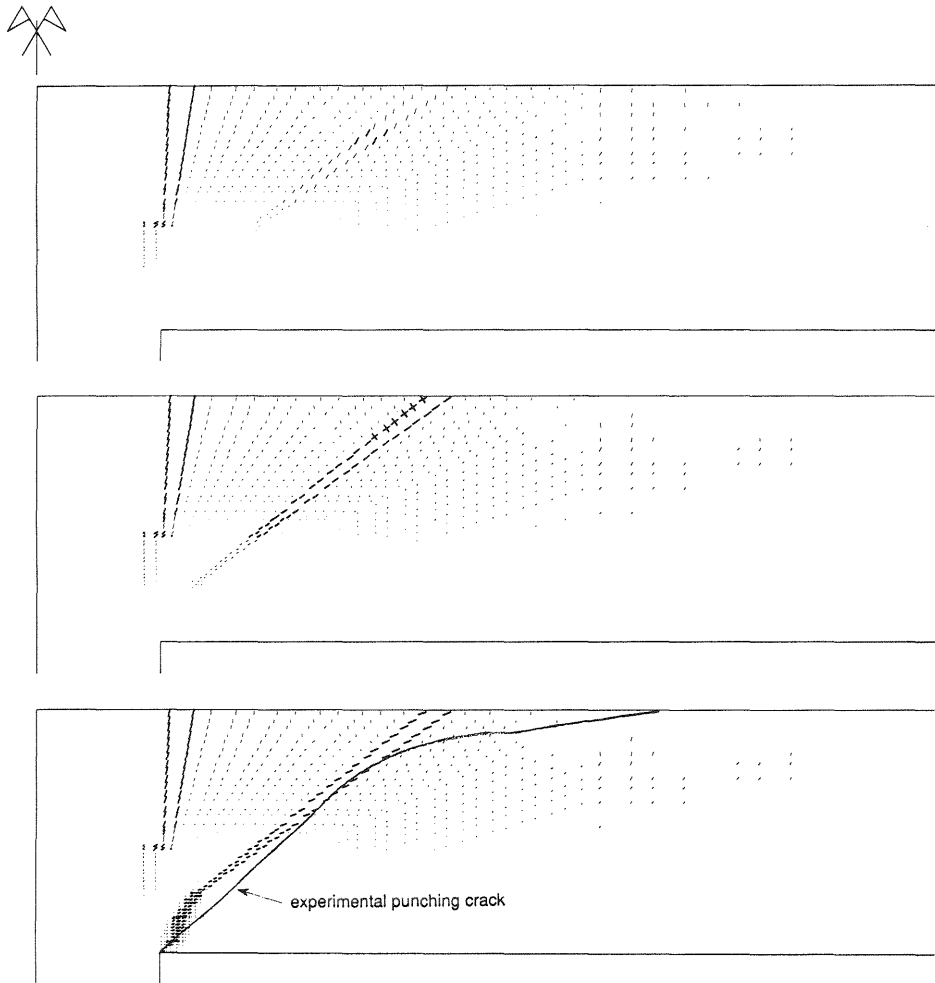
experimental punching crack

Figure 1: Tangential cracks for slab with ring reinforcement; vertical displacement at the extremity: 3.1 mm, 3.2 mm, and 3.3 mm

length is to facilitate some cracks to grow and consequently others to close. This fictitious length is determined by analogy with the crack spacing observed during a tensile test in reinforced concrete.

Four slabs of different sizes with a similar scaling factor which applies to the concrete geometry and the steel area as summarized in table 1 are simulated. Except for these dimensions, the slabs are similar: similar boundary conditions and similar material characteristics. The finite element mesh is refined for large structures to avoid unstable response as the softening slope is controlled by the finite element size. The steel fastening length is constant from one slab to another.

The nominal shear stress given in table 1 is computed so that

$$\tau_n = \frac{P_{punch}}{\pi(2r_s + d)d},\qquad(3)$$

where r_s is the radius of the column, d is the slab effective depth, and P_{punch} is the failure load. It can be observed that the size influences the punching failure as the nominal shear stress decreases with increasing slab thickness.

Table 1: Influence of the size on the punching load and on the nominal shear stress

h	cover	d	r_s	ϕ slab	P_{punch}	τ_n
mm	mm	mm	mm	mm	kN	N/mm^2
75	14.5	60.5	37.5	855	72	2.8
150	29	121	75	1710	222	2.15
300	36.3	264.7	150	3420	737	1.58
450	54.4	396.6	225	5130	1370	1.3

In assuming a constant fracture energy Bažant (1984) derived its size-effect law which is expressed as

$$\tau_n = B(1 + \frac{d}{d_a})^{-\frac{1}{2}},\qquad(4)$$

where B is a constant and d_a is the maximal aggregate size. This law was shown to describe the size-effect in punching failure by Bažant and Cao (1987). Based on the four slab simulations, this size-effect law is adjusted following the RILEM Recommendation (1990) by linear regression which gives

$$\tau_n = 1.55 f_t (1 + \frac{d}{34})^{-1/2}.\qquad(5)$$

1234

This relation is plotted in figure 2 where the two asymptotes: horizontal (strength criterion) and inclined (linear elastic fracture mechanic) are distinguished. Another adjustment of the size-effect
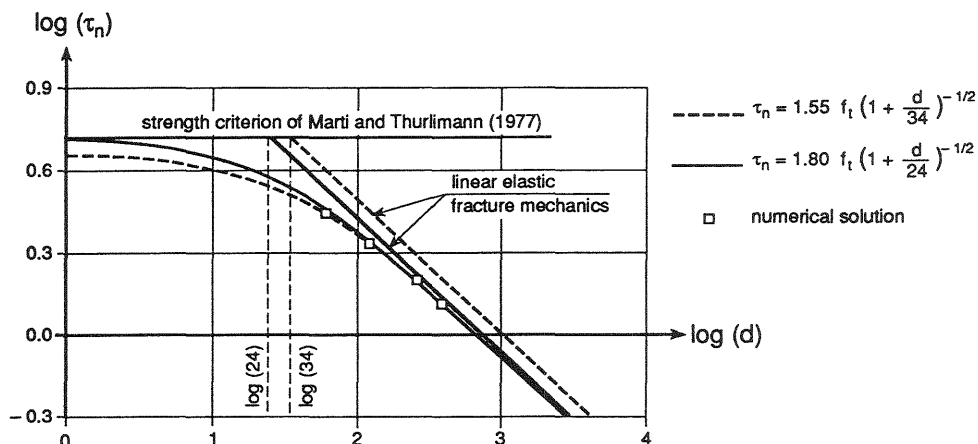

Figure 2: Size-effect law derived from the numerical simulations

law is obtained in forcing the strength criterion given by the upper bound load proposed by Marti and Thurlimann (1977) which is 5.4 N/mm². This leads to the following size-effect law

$$\tau_n = 1.8 f_t (1 + \frac{d}{24})^{-1/2}. \tag{6}$$

This relation is also plotted in figure 2. It can be noted that for both proposed laws, the value d_a is close to standard aggregate size.

The tensile stress distribution along the punching crack just before the crack initiation is presented in figure 3 for three different slabs. It can be clearly observed that the tensile stress distribution is not affine between the three slabs (an affine stress distribution would illustrate an insensitivity with regard to the size of the structure). Therefore, the modification of the tensile stress distribution along the expected punching crack reflects the size-effect.

5   Conclusion

The simulation of punching failure in a circular slab and the comparison with the experimental results reveals that the punching failure mechanism—characterized by a localized inclined punching crack—is generated. This simulation allows to show   that the failure mechanism results from micro-crack coalescence phenomenon
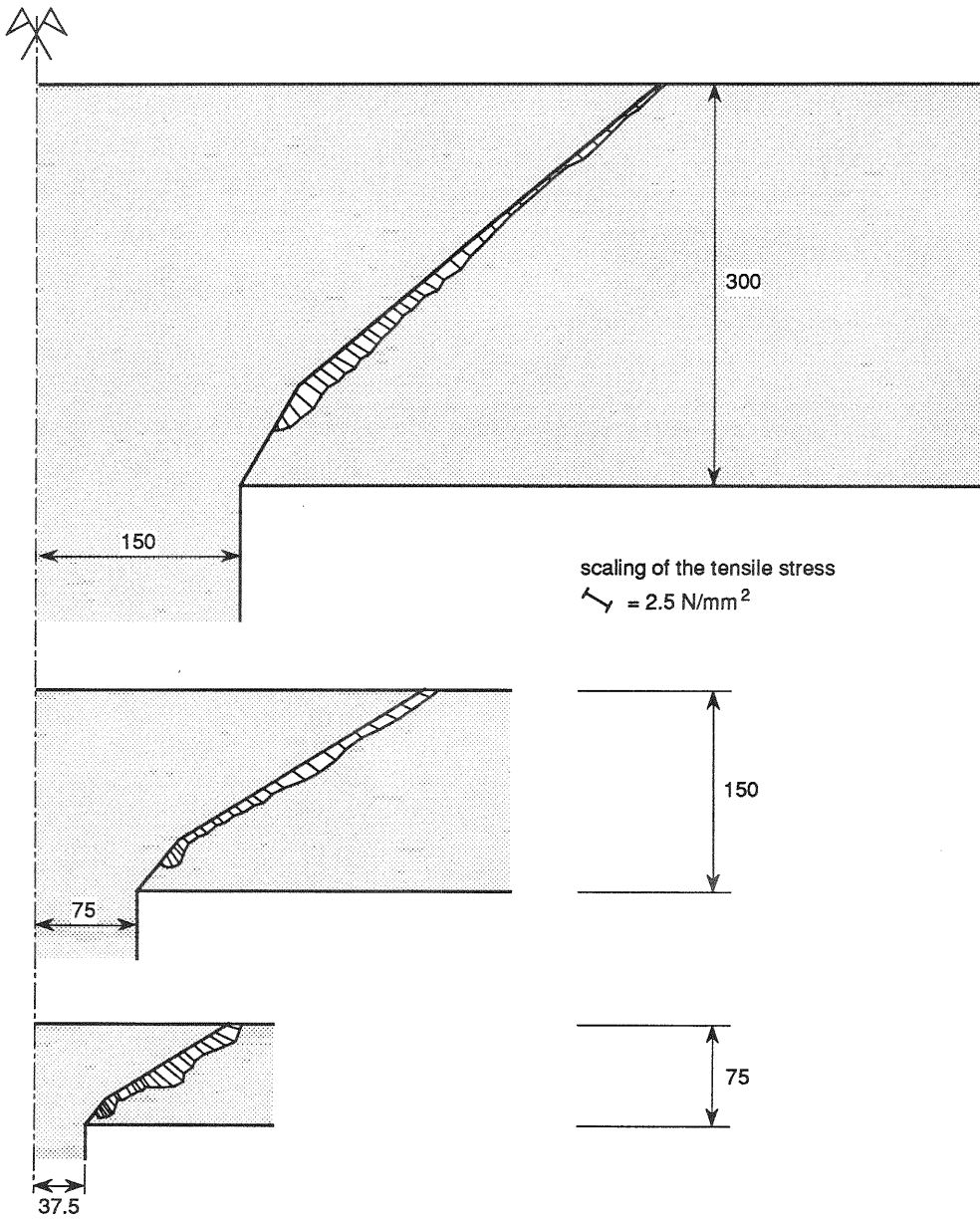
300

150

scaling of the tensile stress

= 2.5 N/mm^2

150

75

75

37.5

Figure 3: Influence of the size on the tensile stress distribution along the punching crack just before the failure initiation

1236

at the top of the slab followed by a crack propagation towards the corner of the slab-column.

The size-effect observed experimentally is reproduced numerically as the nominal shear stress decreases with increasing slab thickness. A size-effect law is adjusted to the numerical results. It is shown that the modification of the tensile stress distribution along the expected punching crack reflects the size-effect.

Acknowledgements

References

Bažant, Z.P. (1984) Size effect in blunt fracture: concrete, rock, metal. **Journal of Engineering Mechanics**, 110(4),518–535.

Bažant, Z.P. (1992), editor. **Fracture mechanics of concrete structures: Part I, State-of-Art Report**. ACI Committee 446, Fracture Mechanics.

Bažant, Z.P. and Cao, Z. (1987) Size effect in punching shear failure of slabs. **ACI Structural Journal**, 84,44–53.

Hillerborg, A., Modeer, M. and Petersson, P.E. (1976) Analysis of crack formation and crack growth in concrete by means of fracture mechanics and finite element. **Cement and Concrete Research (US)**, 6,773–782.

Hughes, T.J.R. (1980) Generalization of selective integration procedures to anisotropic and nonlinear media. **International Journal of Numerical Methods in Engineering**, 15,1413–1418.

Kinnunen, S. and Nylander, H. (1960) Punching of concrete slabs without shear reinforcement. Transactions 158, Royal Institute of Technology, Stockholm.

Lubliner, J., Oliver, J., Oller, S. and Onate, E. (1989) A plastic damage model for concrete. **International Journal of Solids Structures**, 25,299–326.

Marti, P. and Thürlimann, B. (1977) Fliessbedingung für Stahlbeton mit Berücksichtigung der Betonzugfestigkeit. Bericht 67, Institut für Baustatik und Konstruktion ETH Zürich.

Menétrey, Ph. (1994) Numerical analysis of punching failure in reinforced concrete structures. Thesis, Ecole Polytechnique Fédérale de Lausanne.

Menétrey, Ph. and Willam, K.J. (1995) A triaxial failure criterion for concrete and its generalization. **ACI Structural Journal**, 92(2).

Menétrey, Ph., Zimmermann, Th. and Willam, K.J. (1995a) Simulation of punching failure in reinforced concrete. i: computational tool. Rapport IBAP 92.03.5, EPFL. Submitted to the Journal of Structural Engineering, ASCE.

Menétrey, Ph., Walther, R. and Regan, P.E. (1995b) Simulation of punching failure in reinforced concrete. ii: sensitivity analysis. Rapport IBAP 92.03.5, EPFL. Submitted to the Journal of Structural Engineering, ASCE.

Moe, J. (1961) Shearing strength of reinforced concrete slabs and footings under concentrated loads. Bulletin D47, Portland Cement Association.

Ortiz, M. and Simo, J.C. (1986) An analysis of a new class of integration algorithms for elastoplastic constitutive relations. **International Journal of Numerical Methods in Engineering**, 23,353–366.

Regan, P.E. (1983) Punching shear in prestressed concrete slab bridges. Technical report, Engng. Structures Research Group, Polytechnic of Central London.

Regan, P.E. and Braestrup, M.W. (1985) Punching shear in reinforced concrete. **Bulletin d'information** 168, Comité Euro-International du Béton.

RILEM Draft Recommendations (1990) **Size-effect method for determining fracture energy and process zone size of concrete**. Materials and Structures, 23,461–465.